Development of a fully automatic scheme for detection of masses in whole breast ultrasound images

Yuji Ikedo[a)]
Department of Intelligent Image Information, Division of Regeneration and Advanced Medical Sciences, Graduate School of Medicine, Gifu University, 1-1 Yanagido, Gifu 501-1194, Japan

Daisuke Fukuoka
Technology Education, Faculty of Education, Gifu University, 1-1 Yanagido, Gifu 501-1193, Japan

Takeshi Hara and Hiroshi Fujita
Department of Intelligent Image Information, Division of Regeneration and Advanced Medical Sciences, Graduate School of Medicine, Gifu University, 1-1 Yanagido, Gifu 501-1194, Japan

Etsuo Takada
Division of Medical Ultrasonics, Center of Optical Medicine, Dokkyo Medical University, 880 Kitakobayashi, Mibu, Tochigi 321-0293, Japan

Tokiko Endo
Department of Radiology, National Hospital Organization Nagoya Medical Center, 4-1-1 Sannomaru, Naka-ku, Nagoya, Aichi 460-0001, Japan

Takako Morita
Department of Mammary Gland, Chunichi Hospital, 3-6-38 Marunouchi, Naka-ku, Nagoya, Aichi 460-0002, Japan

(Received 22 June 2007; revised 21 August 2007; accepted for publication 15 September 2007; published 23 October 2007)

Ultrasonography has been used for breast cancer screening in Japan. Screening using a conventional hand-held probe is operator dependent and thus it is possible that some areas of the breast may not be scanned. To overcome such problems, a mechanical whole breast ultrasound (US) scanner has been proposed and developed for screening purposes. However, another issue is that radiologists might tire while interpreting all images in a large-volume screening; this increases the likelihood that masses may remain undetected. Therefore, the aim of this study is to develop a fully automatic scheme for the detection of masses in whole breast US images in order to assist the interpretations of radiologists and potentially improve the screening accuracy. The authors database comprised 109 whole breast US images, which include 36 masses (16 malignant masses, 5 fibroadenomas, and 15 cysts). A whole breast US image with 84 slice images (interval between two slice images: 2 mm) was obtained by the ASU-1004 US scanner (ALOKA Co., Ltd., Japan). The feature based on the edge directions in each slice and a method for subtracting between the slice images were used for the detection of masses in the authors proposed scheme. The Canny edge detector was applied to detect edges in US images; these edges were classified as near-vertical edges or near-horizontal edges using a morphological method. The positions of mass candidates were located using the near-vertical edges as a cue. Then, the located positions were segmented by the watershed algorithm and mass candidate regions were detected using the segmented regions and the low-density regions extracted by the slice subtraction method. For the removal of false positives (FPs), rule-based schemes and a quadratic discriminant analysis were applied for the distribution between masses and FPs. As a result, the sensitivity of the authors scheme for the detection of masses was 80.6% (29/36) with 3.8 FPs per whole breast image. The authors scheme for a computer-aided detection may be useful in improving the screening performance and efficiency. [DOI: 10.1118/1.2795825]

Key words: whole breast ultrasound, breast mass, computer-aided detection

I. INTRODUCTION

The incident rate of breast cancer is the highest among all women's cancers in Japan.[1] The detection and treatment of breast cancer at an early stage gives good treatment results; therefore, the early detection of the cancer is an important task for radiologists and surgeons. The two imaging modalities, mammography and ultrasonography, are effective and established methods for the detection of breast masses in breast cancer screening. It has been reported that the use of mammography for breast cancer screening is useful for women aged 40 and above,[2,3] and screening mammography has been an established practice for Japanese women. How-

ever, it is known that mammography is rather limited in dense breasts because small masses might be obscure in dense breast tissues.[4,5] In addition, younger women tend to have dense breasts[6,7] and Asian women tend to have denser ones. However, ultrasonography is capable of detecting masses even in dense breasts, as in the case of young women.[8–10] It has also been reported that breast cancer screening becomes effective when mammography and ultrasonography are used concurrently.[11–14] Hence, ultrasonography has been widely used in Japan for the detection as well as classification of breast masses; further, breast cancer screening by ultrasonography has also been started in some regions.[11] In other words, the importance of breast ultrasonography has been increasing yearly.

Conventional hand-held probes are generally used in ultrasound (US) screening. However, there is a disadvantage in that such US screening is operator dependent. Therefore, the obtained images are poorly reproducible, screening examination takes a long time to scan an entire breast, and some areas of the breast may not be scanned. In order to overcome these problems, several mechanical whole breast US scanners have been developed. For example, ALOKA Co., Ltd., Japan has developed the ASU-1004 whole breast US scanner.[15] This scanner has an automated water path system and scans the entire breast in three overlapping runs. U-systems, Inc. has developed the SomoVu automated breast US system.[16] This system sweeps the breast using a wide-aperture linear transducer. Duric *et al.* have developed a US tomography for breast imaging.[17] The tomography uses a pair of transducers on independent rotation stages such as a transmitter and receiver. The advantages of ultrasonography using such scanners are that the reproducible whole breast images can be easily acquired in a short duration and non-scanning areas are not generated. Due to these advantages, such scanners are effective and can potentially be used as devices for a large-volume screening in the detection of masses. However, the screening will generate a large volume of US images and radiologists might tire while interpreting them. Therefore, it is possible that masses may remain undetected. The screening accuracy might be improved if a computer-aided detection (CAD) system could assist radiologists by indicating the location of mass candidate regions, e.g., mammography with CAD.[18,19]

Several research groups have reported the development of breast ultrasonographic CAD schemes for the detection of masses and their classification as either benign or malignant. Drukker *et al.* have reported an automatic lesion detection technique using a radial gradient index filtering.[20,21] They have also evaluated the performance of their detection and diagnosis method with breast US images obtained using US equipment from two different manufacturers.[22] Horsch *et al.* have attempted to classify masses using a Bayesian neural network or a linear discriminant analysis based on computer-extracted lesion features.[23] Chang *et al.* have proposed a method that uses the watershed segmentation algorithm to find suspicious frames in whole breast US images, which physicians acquired by using a conventional two-dimensional (2D) hand-held probe.[24] They have also reported a mass detection method in whole breast US images[25] and a classification technique that makes use of textural and morphological features.[26] Fukuoka *et al.* have developed a CAD scheme based on active contour model and active balloon model in 2D and three-dimensional (3D) spaces.[27,28] Sahiner *et al.* have investigated the computerized characterization of breast masses in 3D US volumetric images and developed 2D and 3D active contour models for the automated segmentation of the mass volume.[29] Other groups have also suggested classification methods using morphological and texture features or fractal features.[30,31] In addition to the detection and classification of masses, schemes for automatically analyzing the breast density, which is one of the important factors for estimating the risk of breast cancer and its early prevention, have also been reported.[32,33] However, mass detection methods in whole breast US images for a large-volume screening have hardly been reported. Although Chang *et al.* have reported a mass detection method in whole breast US images,[25] their database seems to be small and it is also considered difficult to detect masses with posterior attenuation using their method. Most research does not use whole breast images acquired by a mechanical moving probe; instead, they used 2D images acquired by conventional 2D hand-held probes. Some systems also require a radiologist to manually indicate the locations of masses in images, while others that use segmentation based on the

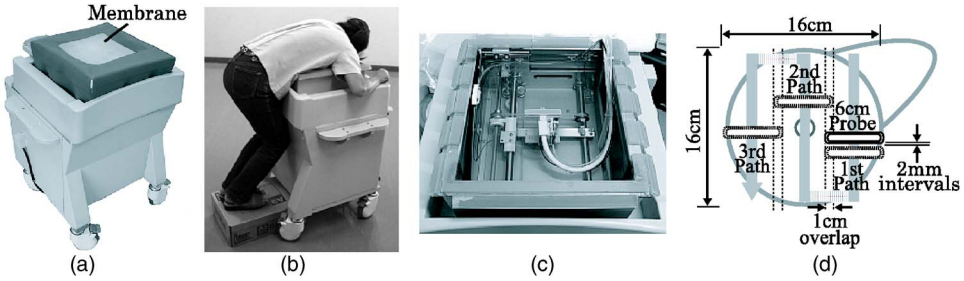

FIG. 1. ASU-1004 whole breast ultrasound scanner. (a) Appearance of the scanner. (b) A subject set her breast on the membrane in a posture of bowing her head. (c) Overhead view removed a membrane. The scanner has a water tank with a linear probe. (d) Scanning process. The probe runs automatically in the tank at 2 mm intervals. An entire breast is scanned 16×16 cm^2 in three overlapping runs.

pixel value and density gradient magnitude may encounter difficulties in detecting masses with obscure boundaries, i.e., with posterior echo attenuation.

We have developed a CAD system for a large-volume breast cancer screening by ultrasonography. The aim of this system is to improve the screening performance and efficiency. The purpose of this study is to propose a fully automatic scheme for the detection of masses in whole breast US images. Our approach differs from others in that we use the feature based on edge directions in the slice images.

II. MATERIALS

II.A. Hardware system overview

An entire breast was scanned by using Prosound-II SSD-5500 US system with the ASU-1004 whole breast US scanner, which are developed by ALOKA Co., Ltd., Japan. The overview of the ASU-1004 mechanism is described in Fig. 1. The US images obtained by this system are in the DICOM format. This scanner has a 6-cm linear transducer (probe) with a frequency range of 5–10 MHz; this probe is immersed in a water tank where it moves mechanically. A special membrane for the US is set on the tank and a subject set her breast on the membrane in a posture of bowing her head. An entire breast can be automatically scanned with an area of 16 $\times$16 cm^2 in three overlapping runs within approximately 30 s. The overlapping has a 1-cm width, as shown in Fig. 1(d), and the interval between two images is 2 mm. A whole breast slice image was generated from the three original images by an integration technique using image processing. The integration technique is described in Sec. III.

II.B. Image database

A whole breast image per breast after applying image integration processing to the original images comprised of 84 slice images with 2 mm intervals. Each slice image matrix had a size of 694$\times$400 pixels; the pixels had a size of 0.23 mm and they had 8-bit gray scale. Our database comprised 109 whole breast images that were obtained in clinical practice and all cases were diagnosed by an experienced radiologist who had 34 years of experience in the field of ultrasonography. Of the 109 whole breast images, 23 were abnormal images and 86 were normal images. These abnormal images included 36 masses (16 malignant masses, 5 fibroadenomas, and 15 cysts) and some images had two or more masses. The size of effective diameters ranged from between 6 and 20 mm, with an average size of 12 mm. The effective diameter implies the diameter of a circle having the same area as a mass. Figure 2 shows the frequency distribution of the mass diameter size.

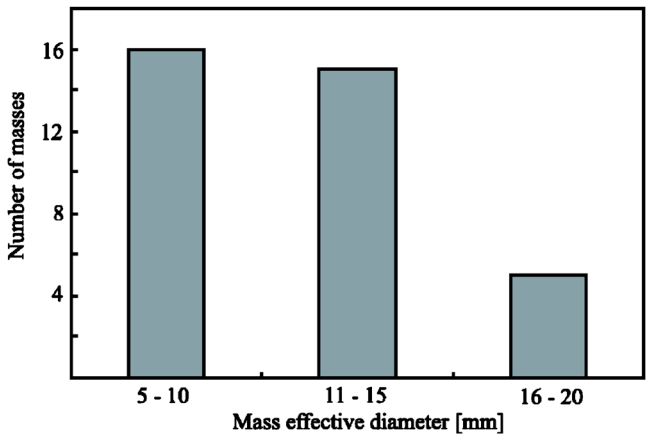

FIG. 2. Histogram of the frequency distribution of mass effective diameter size in our database.

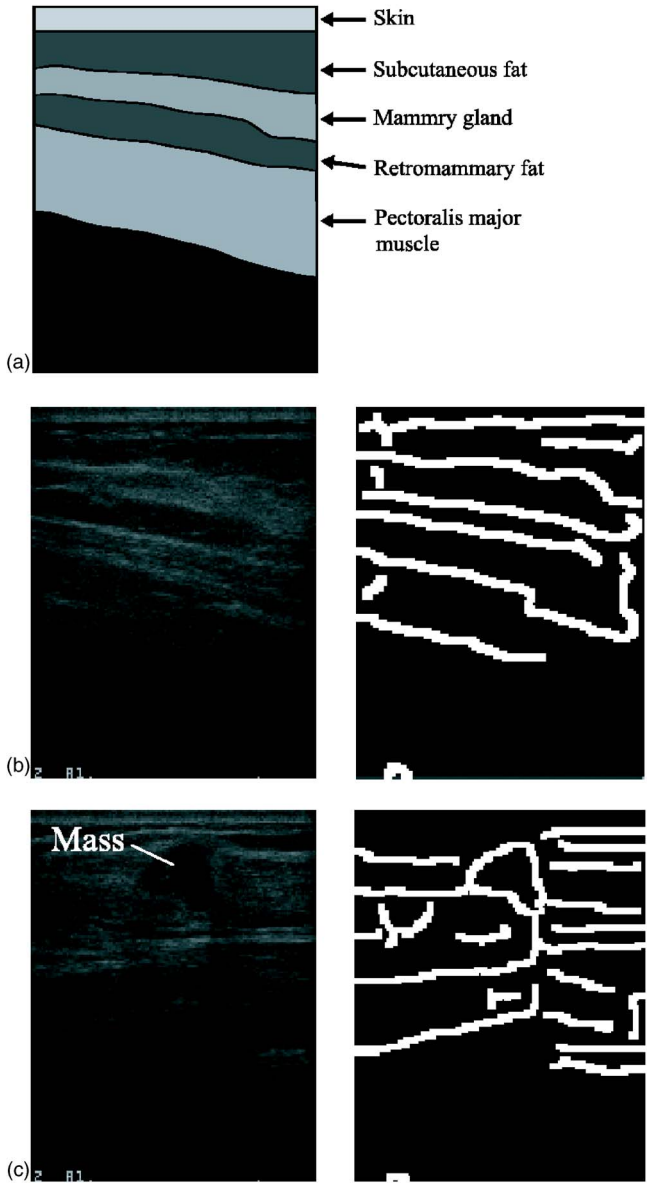

FIG. 3. Breast ultrasound anatomy and clinical breast ultrasound images. (a) Illustration of a breast ultrasound image. Normal breast ultrasound image consists of five main types of tissues. From top to bottom: skin, subcutaneous fat, mammary gland, retromammary fat, and pectoralis major muscle. (b) A normal breast ultrasound image and its edge image. (c) An abnormal breast ultrasound image with a malignant mass and its edge image.

III. METHODS

III.A. Overview

Two features were used for the detection of masses.

The first feature was based on edge directions. A breast US image comprises five main types of tissues, namely skin, subcutaneous fat, mammary gland, retromammary fat, and pectoralis major muscle, as illustrated in Fig. 3(a). An edge image generated from a normal breast US image comprises near-horizontal edges, as shown in Fig. 3(b). However, an edge image generated from an abnormal breast US image with a mass includes near-vertical edges detected in the mass boundary, as shown in Fig. 3(c).

The second feature was based on the density difference between slice images. The idea of using this feature comes from the fact that radiologists interpret all whole breast slice images as a moving image; further, they focus on a region whose density is different as compared to the previous or succeeding slice image.

The flowchart of our detection scheme comprises seven major steps and is shown in Fig. 4.

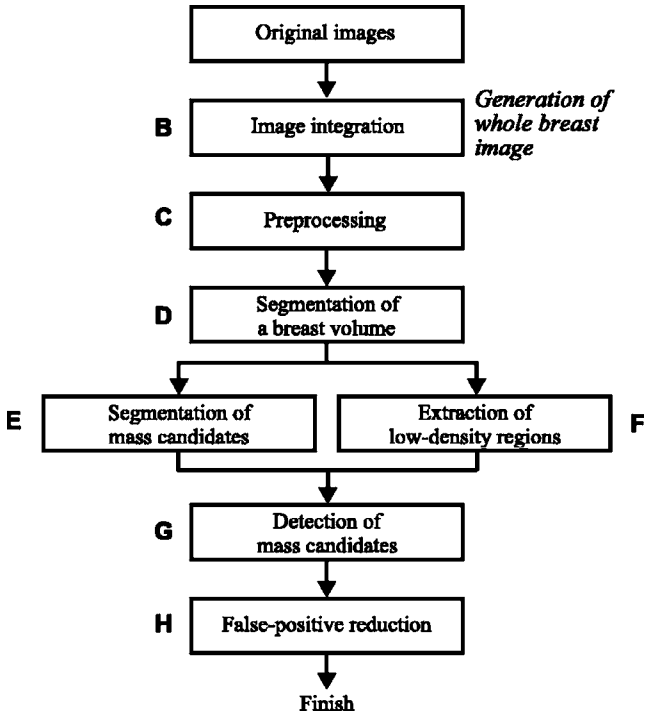

FIG. 4. General overview of the methodology. The original images are integrated to generate a whole breast image (Sec. III B). The whole breast image is preprocessed (Sec. III C) and a breast volume without a skin layer is segmented (Sec. III D). Subsequently, mass candidates are segmented (Sec. III E) and low-density regions are extracted (Sec. III F). Mass candidates are detected based on previous two outputs (Sec. III G). Finally, false positives are reduced (Sec. III H).

III.B. Image integration

A whole breast slice image was generated by integrating three original images. An i^{th} path image is defined as $f_i(x,y)$. The corresponding points in $f_i(x,y)$ and $f_{i+1}(x,y)$ may have a different y coordinate due to the patients' motion such as breathing and heartbeat. Hence, a position adjustment for each image was required in this step.

An integrated slice image $g(x,y)$ is calculated as

$$g(x,y)=\begin{cases} f_i(x,y) & (if(x,y)\in f_i,(x,y)\notin f_{i+1}) \\ f_{i+1}(x,y+\Delta y_{i+1}) & (if(x,y)\notin f_i,(x,y)\in f_{i+1})(i=1,2) \\ \alpha f_i(x,y)+(1-\alpha)f_{i+1}(x,y+\Delta y_{i+1}) & (\text{otherwise}) \end{cases}, \tag{1}$$

where Δy is the adjustment along the y direction and α is the transparency rate, as shown in Fig. 5. The adjustment Δy was computed by a template matching technique that utilizes the overlapped area. A similarity measure R calculated by the sum of the squared difference, as shown in Eq. (2), was used for the matching algorithm.

$$R=\sum_y \sum_x [f_{i+1}(x,y+\Delta y)-f_i(x,y)]^2. \tag{2}$$

A Δy value having a minimum value of R was selected. The transparency rate α was linearly transformed in the range from 0 to 1 based on the relative lateral (x axis) position of two images.

Figure 6 shows the three separate originally acquired images (a) obtained by ASU-1004 and a whole breast slice image (b) integrated by our proposed method. Eventually 84 slice images were generated for each breast; this integration procedure was judged to be successful based on a visual evaluation of all the slices and the cases studied.

III.C. Preprocessing

US images always have a lot of speckle noises that are caused by the interference effects between overlapping echoes, and the image brightness varies with an adjustment in the gain control of a US device. Therefore, noise reduction and image density normalization are used. In this study, impulse noises were removed by applying the median filter; subsequently, minor fluctuating noises were reduced by applying the hysteresis smoothing algorithm.[34] Finally, gray-scale transformation was employed to normalize the image intensity. A preprocessed image obtained after these applying these processes is defined as $h(x,y,z)$.

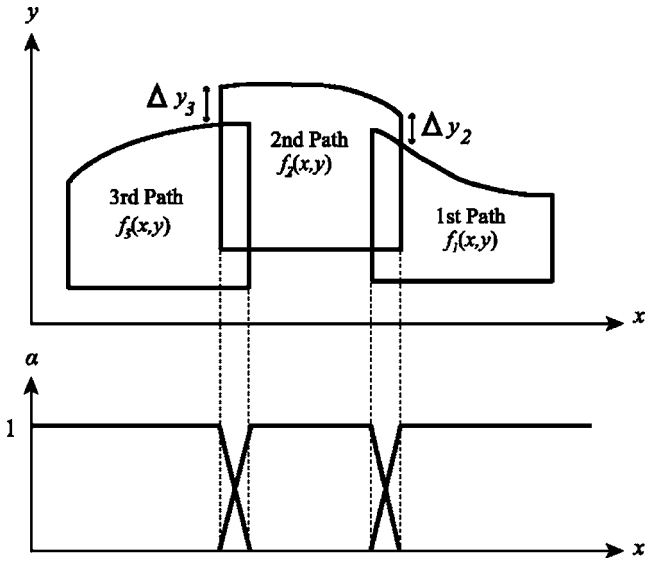

FIG. 5. Positional relations of three separate images (upper part) and transparency rate α of each image (lower part) in the step of image integration.

III.D. Segmentation of a breast volume

As stated previously, features based on edge directions were used for mass detection. Therefore, false positive (FP) regions were generated due to the edges at the boundaries of the skin tissue and subcutaneous fat tissue. In order to reduce such FPs, a breast volume without the skin layer was segmented from each whole breast image.

First, an initial breast volume including the skin volume was extracted from a whole breast image by gray level thresholding with a threshold level of 30, since the breast volume is obviously brighter than its black background. The threshold level was defined empirically. The hole filling technique was applied to the initial breast volume because anechoic masses might be removed by gray level thresholding. The hole filling technique was that holes surrounded by the initial breast volume were included in initial breast volume. The skin tissue was depicted with a high density as compared to other tissues and the skin thickness was less than 5 mm. Gray level thresholding with a threshold level of 180 was applied to the whole breast image. The threshold level was also defined empirically. A volume of 5-mm thickness from the anterior surface of the binary volume was defined as the initial skin volume. The initial skin volume included not only skin tissue but also subcutaneous fat tissue. A skin volume containing only skin tissue was extracted from the initial skin volume using gray level thresholding with a threshold value selected by the discriminant analysis.[35] Finally, the skin volume was removed from the initial breast volume and the remaining volume was defined as a breast volume. Figure 7 shows an example of a slice image of a segmented breast volume.

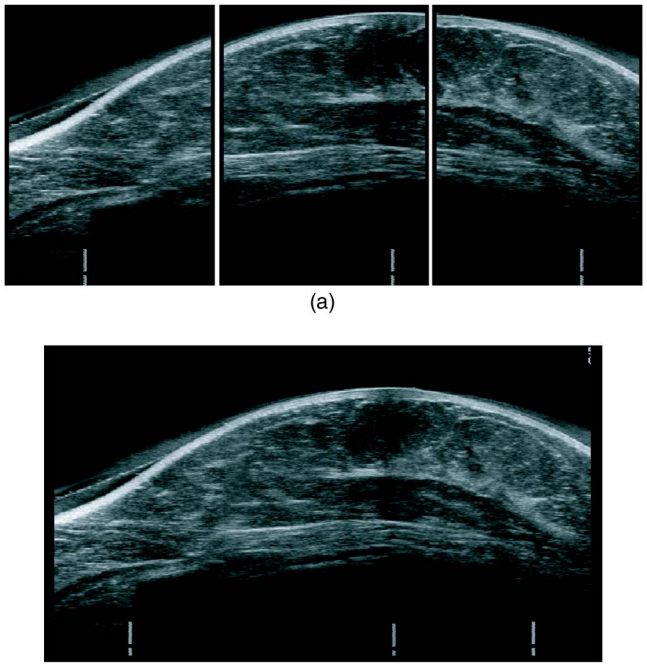

FIG. 6. Example of image integration. (a) Three original images. (b) A whole breast slice image after applying the integration method.

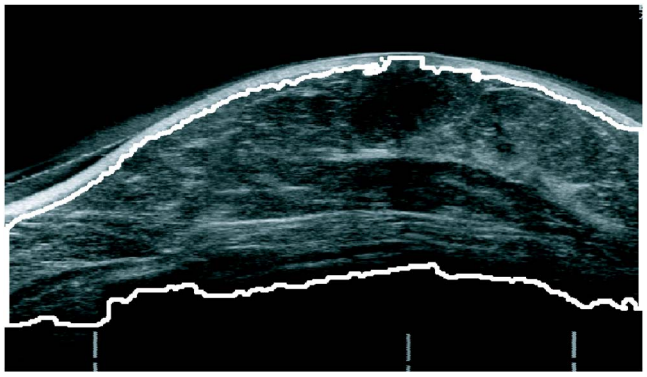

FIG. 7. Example of breast region segmented from a whole breast slice image in Fig. 6(b). Solid line shows the contour of a breast region.

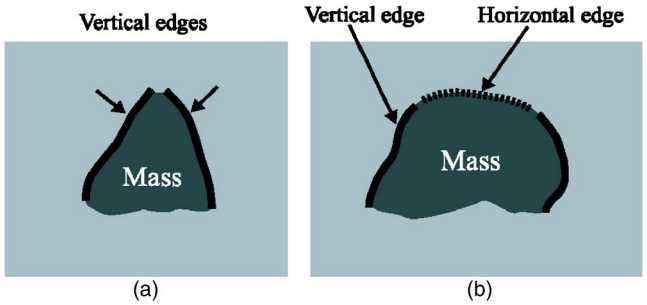

FIG. 8. Illustrations of edges used for the detection of masses. (a) A mass with two near-vertical edges. (b) A mass with two near-vertical and a near-horizontal edges. The near-vertical edges are shown in solid lines and the near-horizontal edge is shown in a dashed line. Near-horizontal edges in the posterior boundary of a mass are not used because there are some masses with posterior echo attenuation.

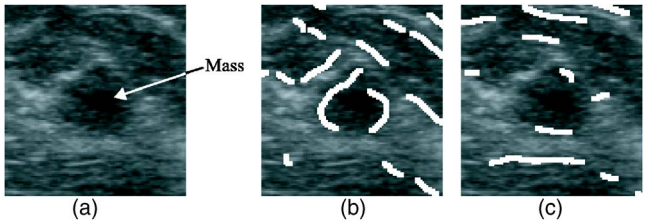

FIG. 9. Example of edge images detected by using our method. (a) Original image with a mass. (b) Near-vertical edge image. (c) Near-horizontal edge image.

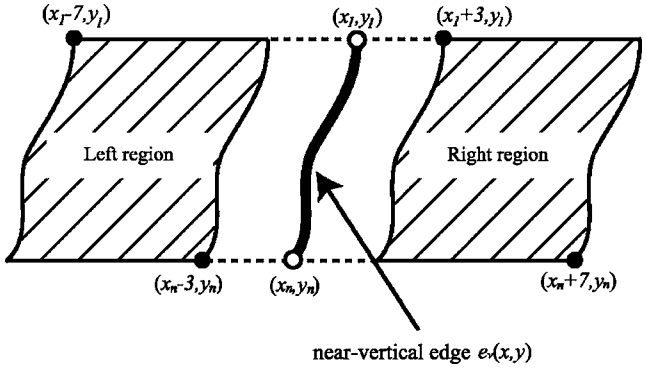

FIG. 10. Illustration of left and right side regions used for the detection of the side with lower density associated with a near-vertical edge $e_v(x,y)$. Average densities in the left side and right side regions are compared.

III.E. Segmentation of mass candidates

Combination of edges (COE), i.e., two near-vertical edges (COE-V) or two near-vertical edges and a single near-horizontal edge (COE-VH), were found near the boundary of a mass region, as shown in Fig. 8. Therefore, a mass candidate could be determined based on the COE-V or COE-VH. Near-horizontal edges in the posterior boundary of a mass were not used because there were some masses with posterior echo attenuation in US images.

Edges in a whole breast slice image were detected by the Canny edge detector[36] and an edge image (EI) was generated by applying a thinning algorithm[37] to the detected edges because the edges detected by the Canny edge detector were not fully thin edges. A near-vertical edge image (n-VEI) was generated by subtracting the EI from a copy of the EI translated along the x direction for two pixels, i.e., $\mathrm{EI}(x,y)>0 \cap \mathrm{EI}(x+2,y)=0$. A near-horizontal edge image (n-HEI) was generated by subtracting the n-VEI from the EI, i.e., $\mathrm{EI}(x,y)>0 \cap n\text{-VEI}(x,y)=0$. Figure 9 shows an example image of n-VEI and n-HEI. The side with a lower density associated with each near-vertical edge was determined by comparing the average densities in the left and right side regions, as shown in Fig. 10. Both regions were kept at a distance three pixels (along the x axis) away from the near-vertical edge because they reduce the effect of the neighborhood densities of the near-vertical edge. Consider that the average density in the right side region of a near-vertical edge is lower than that in the left side region; region of interest 1 (ROI1) was defined as shown in Fig. 11(a). With regard to the top pixel (x_1,y_1) of the near-vertical edge, ROI1 is constructed at the top left hand corner located at (x_1+1,y_1+4) with a size of 9×9 pixels. If another near-vertical edge exists in ROI1, a COE-V scenario was established. If a near-horizontal edge exists in ROI1 and another near-vertical edge exists in ROI2, as shown in Fig. 11(b), a COE-VH scenario was established. With regard to the left pixel (x_1,y_1) and the right pixel (x_n,y_n) of the near-horizontal edge and the height H of the first near-vertical edge, ROI2 is constructed at the top left hand corner located at (x_1,y_1) and at the bottom right hand corner located at (x_n+5,y_n-H). A near-vertical edge with no other edges found in ROI1 or ROI2 was eliminated from the n-VEI. ROI3 was constructed for the near-vertical edges where a COE-V or COE-VH scenario had been established, as shown in Fig. 11(c). Referring the top pixel (x_1,y_1), right pixel (x_i,y_i), left pixel (x_j,y_j), and bottom pixel (x_n,y_n) of the near-vertical edge, ROI3 is constructed at the top left hand corner located at (x_j-21,y_1+21) and at the bottom right corner located at (x_i+86,y_n-21). ROI3 was segmented by the watershed algorithm.[38,39] If the average density of a segmented region was higher than that of ROI3, the segmented

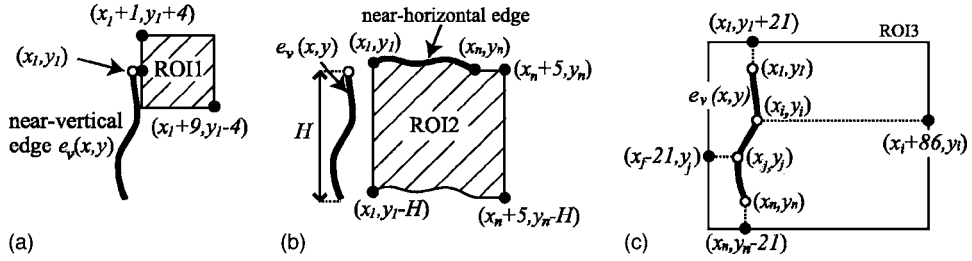

FIG. 11. Illustration of region of interest (ROI) used for the detection of a near-vertical or a near-horizontal edges in neighborhood of a near-vertical edge $e_v(x,y)$. In all illustrations, consider that the average density in the right side region of the $e_v(x,y)$ is lower that in the left side region. If the average density in the left side region is lower, the ROIs are set to the left side of $e_v(x,y)$. (a) Definition of ROI1. With regard to the top pixel (x_1,y_1) of $e_v(x,y)$, the ROI1 is constructed at the top left hand corner located at (x_1+1,y_1+4) with a size of 9×9 pixels. (b) Definition of ROI2. With regard to the left pixel (x_1,y_1) and the right pixel (x_n,y_n) of the near-horizontal edge, and the height H of $e_v(x,y)$, the ROI2 is constructed at the top left hand corner located at (x_1,y_1) and at the bottom right hand corner located at (x_n+5,y_n-H). (c) Definition of ROI3. With regard to the top pixel (x_1,y_1), right pixel (x_i,y_i), left pixel (x_j,y_j), and bottom pixel (x_n,y_n) of $e_v(x,y)$, the ROI3 is constructed at the top left hand corner located at (x_j-21,y_1+21) and at the bottom right corner located at (x_i+86,y_n-21). The 86 and 21 pixels correspond to 20 and 5 mm, respectively.

region was removed. Contiguous regions were stitched, and the maximum size region was extracted from ROI3 as a mass candidate.

III.F. Extraction of low-density regions

If the pixel density in a current slice image is lower than that of the same pixel in a previous slice image, the pixel in the current slice image is defined as a low-density pixel. Low-density regions comprise low-density pixels.

The following method was applied twice, once to the slice forward and once to the slice backward. First, a boundary pixel between a low-density pixel and a high-density pixel was detected by the slice subtraction method. The boundary pixel (i,j,k) is given by

$$h(i,j,k-1)-h(i,j,k+1)>30, \tag{3}$$

where the threshold value of 30 is selected empirically. If a boundary pixel is detected, a low-density pixel is given by

$$h(i,j,k-1)-h(i,j,k+i)>30(i=1,\ldots,5), \tag{4}$$

where i is less than or equal to 5 because the maximum radius of the masses in our database is 10 mm and the slice interval is 2 mm. In the second time (slice backward), $k-1$, $k+1$, and $k+i$ were replaced by $k+1$, $k-1$, and $k-i$, respectively, in the method and the same method was applied again.

III.G. Detection of mass candidates

An area of an extracted region (ER) in Sec. III E is denoted by AER. If the area of a low-density region included in the ER was greater than or equal to eight tenths of the AER, the ER was detected as an initial mass candidate region. Figure 12 shows an example of an extracted mass region in an ultrasound image.

III.H. False positive reduction

III.H.1. Feature extraction

In this study, FP candidates were reduced employing two methods, i.e., rule-based (RB) technique and quadratic discriminant analysis[40] (QDA). These methods were performed using five features including area (A), average density (AD), position of center of gravity (PCG), difference of average density (DAD), and depth-to-width ratio (DWR) for each candidate region in a slice image. A is the number of pixels in a mass candidate region and AD is the average density in the candidate region. PCG is the distance between the center of gravity and the posterior boundary of the breast region in the same x coordinate as the center of gravity, as shown in Fig. 13. DAD is given by subtracting the average density of the core region from that of the periphery region, as shown in Fig. 14. The core region was generated by applying "morphological erosion"[41] with a structuring element of a 5×5 circle to the candidate region. The periphery region was generated by subtracting the candidate region from the expanded region by applying "morphological dilation"[41] with a structuring element of a 9×9 circle to the candidate region. However, in this process, the candidate region was expanded by morphological dilation with a structuring element of a 5×5 circle to reduce the effect of the candidate margin density. Only the anterior side region of the center of gravity was used in both the core and the periphery regions in order to eliminate the effect of posterior echo attenuation. DWR is the aspect ratio of a rectangle outlining a mass candidate region.

The distributions of the five features are plotted in Fig. 15 and the results of tests for the univariate equality of group

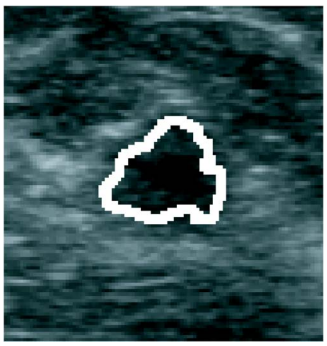

FIG. 12. Detection of the mass shown in Fig. 9(a).

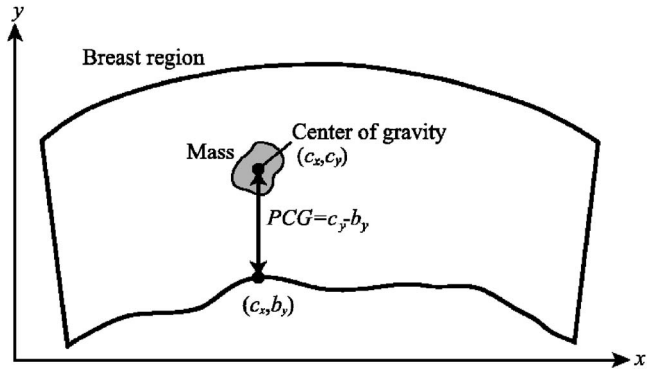

FIG. 13. Definition of the position of center of gravity (PCG). PCG is the distance between the center of gravity (c_x,c_y) of a mass region and the posterior boundary of the breast region (c_x,b_y).

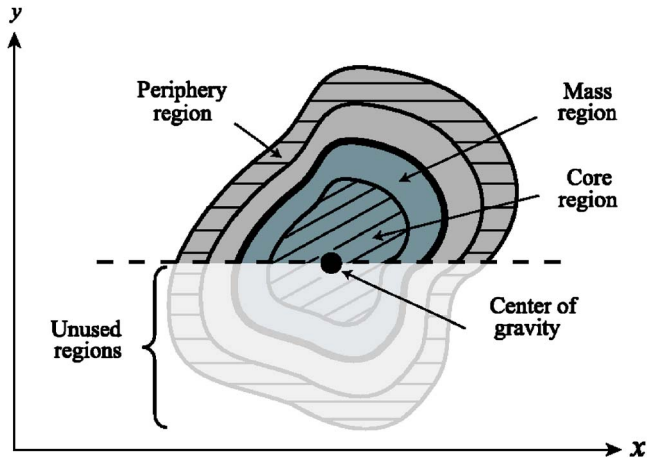

FIG. 14. Illustration of the core and periphery regions which are used to calculate a DAD.

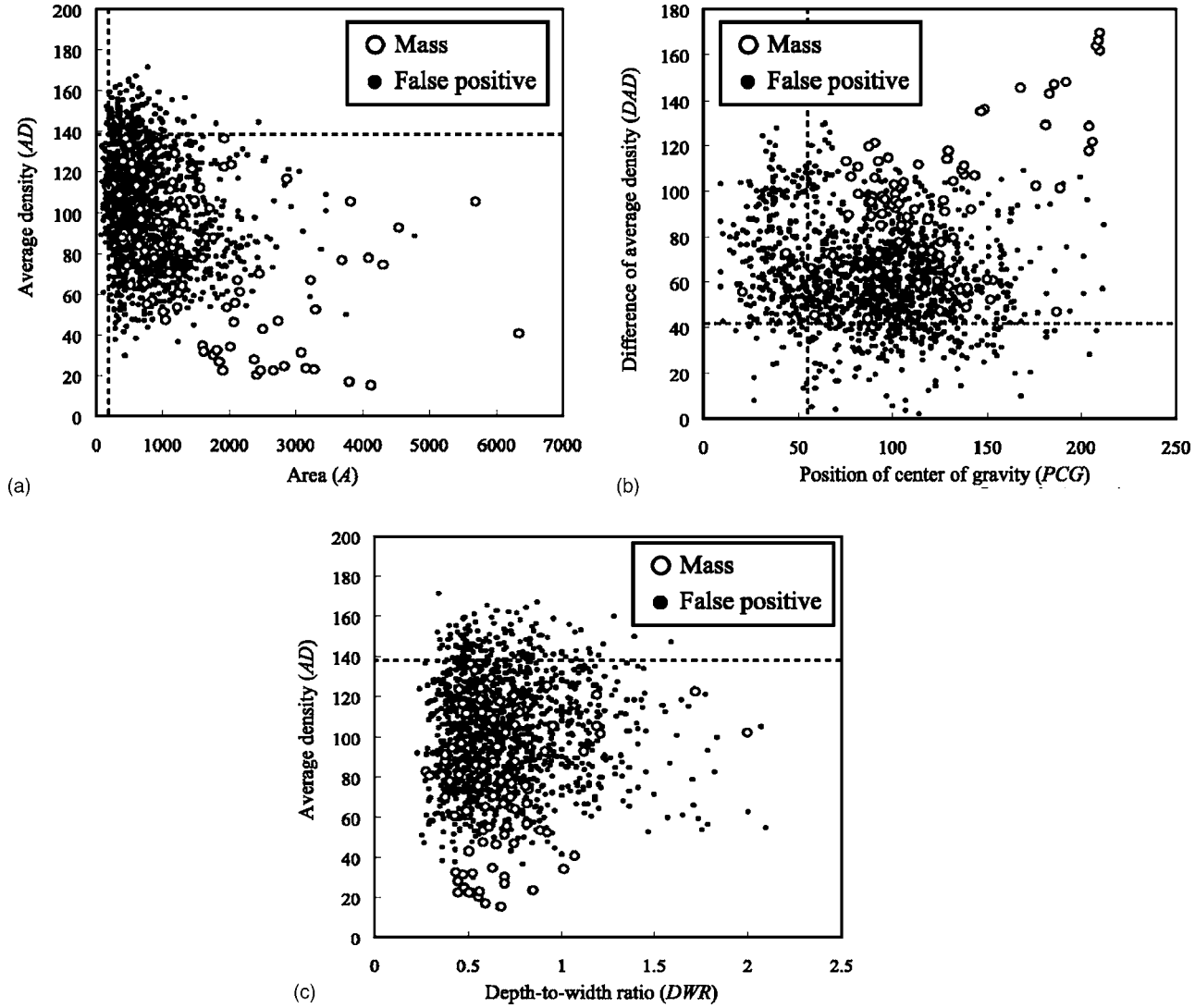

FIG. 15. Distribution of four features in each mass candidate region (mass: circle; false positive: dot). (a) Area vs average density. (b) Position of center of gravity vs difference of average density. The dotted lines indicate the thresholds for reduction of false positives. (c) Depth-to-width ratio vs average density. The dotted lines in each figure indicate the threshold values using rule-based techniques.

means are shown in Table I. Wilks' lambda[42] is defined as the ratio of within-group variance to the total variance and indicates the degree of discrimination between the masses and FPs; for A, this value was lesser than that for any other feature. The F value[42] for A was also higher than that for any other feature. This result indicates that A greatly contributed in distinguishing between masses and FPs. DWR contributed to some extent in eliminating FPs, because DWR was an only shape feature. Therefore, DWR was used as a parameter to reduce FPs in this study.

TABLE I. Test for univariate equality of group means in distinguishing between masses and FPs (A: area, AD: average density, PCG: position of center of gravity, DAD: difference of average density, and DWR: depth-to-width ratio).

Feature	Wilk's lambda	F value	P value
A	0.965	201.910	<0.001
AD	0.989	62.895	<0.001
PCG	0.993	40.957	<0.001
DAD	0.967	188.868	<0.001
DWR	1.000	0.504	0.478

III.H.2. Rule-based technique

Four features, namely, A, AD, PCG, and DAD were used for the RB technique. We applied the RB technique to these feature diagrams by drawing dotted lines, as shown in Figs. 15(a) and 15(b), and the candidate regions in the feature spaces, with the A value greater than or equal to 200, the AD value less than or equal to 137, the PCG value greater than or equal to 57, and the DAD value greater than or equal to 43, remained as mass candidates. However, two masses were removed by the PCG rule [see Fig. 15(b)]. The feature values of the masses lied outside the distribution of other masses

and the same masses were detected in other slices. Therefore, it is considered that no problems occur by removing these two mass regions.

Those threshold values were decided for our database. If unknown new images were used for our proposed method, masses out of the threshold values were removed by the RB technique. In that case, the threshold values might be needed to reconsider.

III.H.3. Quadratic discriminant analysis

All features of the mass candidate volumes were used for the QDA. However, the volume of a mass candidate region was determined in all slice images. Therefore, in this part, each feature of a mass candidate volume was defined as an average feature value of all mass candidate regions in order to construct the mass candidate volume. The quadratic discriminant function is defined by

$$h(\mathbf{X}) = \frac{1}{2}(\mathbf{X}-\mathbf{M}_L)^T\sum_L^{-1}(\mathbf{X}-\mathbf{M}_L) - \frac{1}{2}(\mathbf{X}-\mathbf{M}_F)^T\sum_F^{-1}(\mathbf{X}-\mathbf{M}_F) + \frac{1}{2}\log\frac{|\mathbf{\Sigma}_L|}{|\mathbf{\Sigma}_F|}, \quad (5)$$

where $\boldsymbol{X}$ is a feature vector of all candidates. $(\mathbf{M}_L, \mathbf{\Sigma}_L)$ and $(\mathbf{M}_F, \mathbf{\Sigma}_F)$ are the mean feature vectors and covariance matrix of the features in the mass candidates and the FPs, respectively.

Employing the RB technique before applying QDA might be effective for the accurate calculation of the QDA decision boundary because outlying FPs were removed using the RB technique.

IV. RESULTS AND DISCUSSION

The proposed scheme for the detection of masses was evaluated using our database. In this study, the resubstitution method[43] was utilized for the evaluation. The resubstitution method is that the same data set is used, first for training and then for testing. This was because our database was small and there were not many masses. If the center of gravity of a detected region is located in a mass region, the detected region is considered to be true positive. The sensitivities of the detection of masses before and after applying the RB technique for FP reduction were 91.7% (33/36) with 35.8 FPs (3905/109) and 91.7% (33/36) with 22.5 FPs (2448/109) per whole breast image, respectively. However, the sensitivity with QDA was 80.6% (29/36) with 3.8 FPs (409/109) per whole breast image. In addition, the leave-one-out method was also employed to evaluate the performance of the scheme. The sensitivity with QDA was 80.6% (29/36) with 6.6 FPs (723/109) per whole breast image. Figure 16 shows the FROC curves[44] for the overall performance of our detection scheme as evaluated by the resubstitution and leave-one-out methods. This curve was determined by changing the threshold level of the output value of the quadratic discriminant function. The evaluation using the leave-one-out method could be underestimated because our database was small. Therefore, in future studies, we need to evaluate the detection scheme using a large database by the leave-one-out method and a cross validation method.

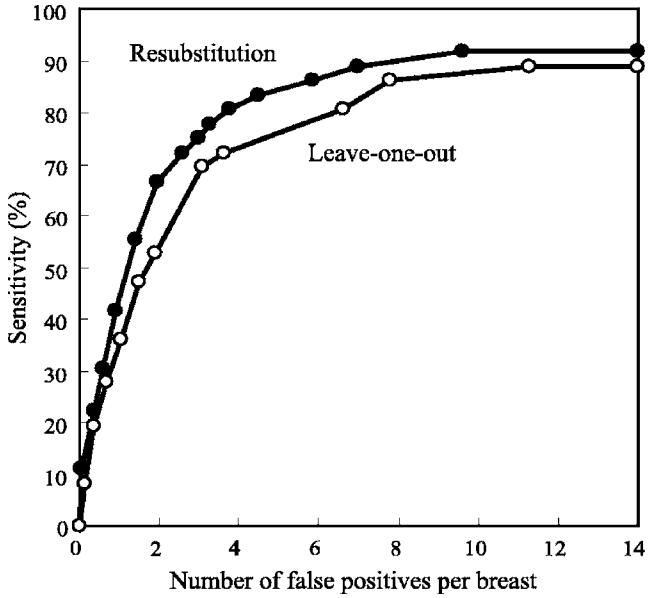

FIG. 16. FROC curves for overall performance of our scheme for the detection of masses evaluated by the resubstitution and leave-one-out methods (resubstitution: solid line with black circle; leave-one-out: solid line with white circle).

We found that the feature based on edge directions was useful for the detection of masses. It is also easy to apply the detection scheme to 2D US images obtained by a conventional hand-held probe because the scheme employs a 2D method and not a 3D method. This scheme could detect masses effectively even if they had posterior attenuation. On the other hand, it was difficult to detect flat-shaped masses (short in the vertical dimension and long in the horizontal dimension when viewed on a slice image) because the near-vertical edges of the masses could not be easily detected, as shown in Fig. 17(a).

A lot of FPs were generated at an initial detection stage, many of which remained even after applying the reduction procedures for FPs. These remaining FPs corresponded to the fat and rib regions, as shown in Figs. 17(b) and 17(c). This is because the edges of Cooper's ligaments in the fat tissue and rib section were incorrectly detected. However, there is a difference between the 3D shapes of the masses and fat tissue or ribs. Masses are spherical, while the fat tissue and ribs are not. The 3D characteristics were not used in our proposed detection method because the interval of slice images in our database was large (2 mm). However, the ASU-1004 has now been improved to scan an entire breast with interval of 2 mm or less and the 3D shape characteristics can be extracted easily. Therefore, it seems that the introduction of a 3D method for the detection of masses is one of the effective methods for solving such a problem.

We expect that in the future, the use of our whole breast US images will lead to the development of other CAD systems such as the quantitative evaluation of breast densities

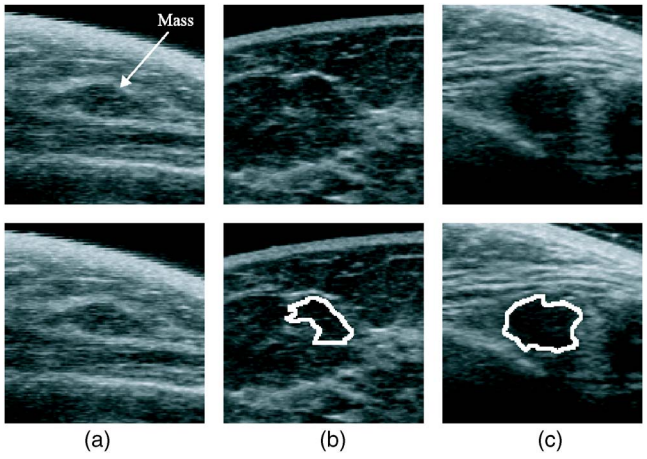

FIG. 17. Example of a false negative and two false positives. Upper row: original images. Lower row: result images. (a) False negative image with a mass (fibroadenoma). (b) False positive image. The detected region was fat tissues with Copper's ligaments. (c) False positive image. The detected region was a rib region.

and the analysis of architectural distortions. Furthermore, it may also be possible to detect interval changes using the image registration technique of previous and current whole breast images.

V. CONCLUSION

We have developed a fully automatic scheme for the detection of masses in whole breast US images. Using our scheme, the sensitivity of the detection of masses was 80.6% (29/36) with 3.8 FPs (409/109) per whole breast image. We found that the feature based on edge directions is useful for the detection of masses in US images. A CAD system employing our proposed scheme may be useful in improving the screening performance and efficiency.

ACKNOWLEDGMENTS

This work was supported in part by a grant for the Knowledge Cluster Gifu-Ogaki, referred to as the "Robotics Advanced Medical Cluster," from the Ministry of Education, Culture, Sports, Science and Technology, Japan. The authors are grateful to ALOKA Co., Ltd., Japan and TAK Co., Ltd., Japan for their assistance in this study. The authors thank Gobert Lee, Ph.D. and Yoshikazu Uchiyama, Ph.D. for their helpful comments and discussions. The authors also thank the members of Fujita Laboratory at Gifu University for their helpful advice.

[a]Author to whom correspondence should be addressed. Telephone: +81-58-230-6519; Fax: +81-58-230-6514. Electronic address: ikedo@fjt.info.gifu-u.ac.jp

[1]Y. Minami, Y. Tsubono, Y. Nishino, N. Ohuchi, D. Shibuya, and S. Hisamichi, "The increase of female breast cancer incidence in Japan: Emergence of birth cohort effect," Int. J. Cancer **108**, 901–906 (2004).
[2]S. A. Norman, A. R. Localio, L. Zhou, A. L. Weber, R. J. Coates, K. E. Malone, L. Bernstein, P. A. Marchbanks, J. M. Liff, N. C. Lee, and M. R. Nadel, "Benefit of screening mammography in reducing the rate of late-stage breast cancer diagnoses (United States)," Cancer Causes Control **17**, 921–929 (2006).
[3]L. L. Humphrey, M. Helfand, B. K. S. Chan, and S. H. Woolf, "Breast cancer screening: A summary of the evidence for the US preventive services task force," Ann. Intern. Med. **137**, 347–360 (2002).
[4]H. M. Zonderland, E. G. Coerkamp, M. J. Van de Vijver, and A. E. Van Voorthuisen, "Diagnosis of breast cancer: Contribution of US as an adjunct to mammography," Radiology **213**, 413–422 (1999).
[5]R. D. Rosenberg, W. C. Hunt, M. R. Williamson, F. D. Gilliland, P. W. Wiest, C. A. Kelsey, C. R. Key, and M. N. Linver, "Effects of age, breast density, ethnicity, and estrogen replacement therapy on screening mammographic sensitivity and cancer stage at diagnosis: Review of 183,134 screening mammograms in Albuquerque, New Mexico," Radiology **209**, 511–518 (1998).
[6]M. S. Soo, E. L. Rosen, J. A. Baker, T. T. Vo, and B. A. Boyd, "Negative predictive value of sonography with mammography in patients with palpable breast lesions," AJR, Am. J. Roentgenol. **177**, 1167–1170 (2001).
[7]K. Kerlikowske, D. Grady, J. Barclay, E. A. Sickles, and V. Ernster, "Effect of age, breast density, and family history on the sensitivity of first screening mammography," JAMA, J. Am. Med. Assoc. **276**, 33–38 (1996).
[8]I. Leconte, C. Feger, C. Galant, M. Berlière, B. V. Berg, W. D'Hoore, and B. Maldague, "Mammography and subsequent whole-breast sonography of nonpalpable breast cancers: The importance of radiologic breast density," AJR, Am. J. Roentgenol. **180**, 1675–1679 (2003).
[9]S. S. Kaplan, "Clinical utility of bilateral whole-breast US in the evaluation of women with dense breast tissue," Radiology **221**, 641–649 (2001).
[10]T. Osako, K. Takahashi, T. Iwase, K. Iijima, Y. Miyagi, S. Nishimura, K. Tada, M. Makita, F. Akiyama, G. Sakamoto, and F. Kasumi, "Diagnostic ultrasonography and mammography for invasive and noninvasive breast cancer in women aged 30 to 39 years," Breast Cancer **14**, 229–233 (2007).
[11]H. Morikubo, "Breast cancer screening by palpation, ultrasound, and mammography," in *Research and Development in Breast Ultrasound*, edited by E. Ueno, T. Shiina, M. Kubota, and K. Sawai (Springer, Tokyo, 2005), pp. 159–162.
[12]T. M. Kolb, J. Lichy, and J. H. Newhouse, "Comparison of the performance of screening mammography, physical examination, and breast US and evaluation of factors that influence them: An analysis of 27,825 patient evaluations," Radiology **225**, 165–175 (2002).
[13]K. Flobbe, P. J. Nelemans, A. G. H. Kessels, G. L. Beets, M. F. von Meyenfeldt, and J. M. A. van Engelshoven, "The role of ultrasonography as an adjunct to mammography in the detection of breast cancer: A systematic review," Eur. J. Cancer **38**, 1044–1050 (2002).
[14]D. B. Kopans, "Breast-cancer screening with ultrasonography," Lancet **354**, 2096–2097 (1999).
[15]E. Takada, Y. Ikedo, D. Fukuoka, T. Hara, H. Fujita, T. Endo, and T. Morita, "Semi-automatic ultrasonic full-breast scanner and computer-assisted detection system for breast cancer mass screening," Proc. SPIE **6514**, 65141T-1–65141T-10 (2007).
[16]U-systems, http://www.u-sys.com.
[17]N. Duric, P. Littrup, A. Babkin, D. Chambers, S. Azevedo, A. Kalinin, R. Pevzner, M. Tokarev, E. Holsapple, O. Rama, and R. Duncan, "Development of ultrasound tomography for breast imaging: Technical assessment," Med. Phys. **32**, 1375–1386 (2005).
[18]T. W. Freer and M. J. Ulissey, "Screening mammography with computer-aided detection: Prospective study of 12,860 patients in a community breast center," Radiology **220**, 781–786 (2001).
[19]M. A. Helvie *et al.*, "Sensitivity of noncommercial computer-aided detection system for mammographic breast cancer detection: Pilot clinical trial," Radiology **231**, 208–214 (2004).
[20]K. Drukker, M. L. Giger, K. Horsch, M. A. Kupinski, and C. J. Vyborny, "Computerized lesion detection on breast ultrasound," Med. Phys. **29**, 1438–1446 (2002).
[21]K. Drukker, M. L. Giger, C. J. Vyborny, and E. B. Mendelson, "Computerized detection and classification of cancer on breast ultrasound," Acad. Radiol. **11**, 526–535 (2004).
[22]K. Drukker, M. L. Giger, and C. E. Metz, "Robustness of computerized lesion detection and classification scheme across different breast US platform," Radiology **237**, 834–840 (2005).
[23]K. Horsch, M. L. Giger, L. A. Venta, and C. J. Vyborny, "Computerized diagnosis of breast lesions on ultrasound," Med. Phys. **29**, 157–164 (2002).
[24]R. F. Chang, K. C. Chang-Chien, H. J. Chen, D. R. Chen, E. Takada, and W. K. Moon, "Whole breast computer-aided screening using free-hand ultrasound," in CARS2005: Computer Assisted Radiology and Surgery

2005, edited by H. U. Lemke, K.Inamura, K. Doi, M. W. Vannier, and A. G. Farman, 2005, pp. 1075–1080.
[25]R. F. Chang, C. J. Chen, E. Takada, C. M. Kuo, and D. R. Chen, "Image stitching and computer-aided diagnosis for whole breast ultrasound image," in CARS2006: Computer Assisted Radiology and Surgery 2006, edited by H. U. Lemke, K. Inamura, M. W. Vannier, and A. G. Farman, 2006, Vol. 1, Supp. 1, pp. 340–343.
[26]R. F. Chang, C. L. Tsai, S. F. Huang, W. J. Kuo, D. R. Chen, W. K. Moon, Y. L. Huang, W. M. Chen, and W. J. Wu, "Computer-aided diagnosis for 2D/3D breast ultrasound," in *Recent Advances in Breast Imaging, Mammography, and Computer-Aided Diagnosis of Breast Cancer*, edited by J. S. Suri and R. M. Rangayyan (SPIE, Bellingham, WA, 2006), pp. 569–612.
[27]D. Fukuoka, T. Hara, H. Fujita, T. Endo, and Y. Kato, "Automated detection and classification of masses on breast ultrasonograms and its 3D imaging technique," in *IWDM2000: 5th International Workshop on Digital Mammography*, edited by M. J. Yaffe (Medical Physics, Madison, WI, 2001), pp. 182–188.
[28]D. Fukuoka, T. Hara, and H. Fujita, "Detection, characterization, and visualization of breast cancer using 3D ultrasound images," in *Recent Advances in Breast Imaging, Mammography, and Computer-Aided Diagnosis of Breast Cancer*, edited by J. S. Suri and R. M. Rangayyan (SPIE, Bellingham, WA, 2006), pp. 557–567.
[29]B. Sahiner, H. P. Chan, M. A. Roubidoux, M. A. Helvie, L. M. Hadjiiski, A. Ramachandran, C. Paramagul, G. L. LeCarpentier, A. Nees, and C. Blane, "Computerized characterization of breast masses on three-dimensional ultrasound volumes," Med. Phys. **31**, 744–754 (2004).
[30]R. Sivaramakrishna, K. A. Powell, M. L. Lieber, W. A. Chilcote, and R. Shekhar, "Texture analysis of lesions in breast ultrasound images," Comput. Med. Imaging Graph. **26**, 303–307 (2002).
[31]A. V. Alvarenga, W. C. A. Pereira, A. F. C. Infantosi, and C. M. Azevedo, "Complexity curve and grey level co-occurrence matrix in the texture evaluation of breast tumor on ultrasound images," Med. Phys. **34**, 379–387 (2007).
[32]C. Glide, N. Duric, and P. Littrup, "Novel approach to evaluating breast density utilizing ultrasound tomography," Med. Phys. **34**, 744–753 (2007).
[33]R. F. Chang, K. C. Chang-Chien, E. Takada, J. S. Suri, W. K. Moon, J. H. K. Wu, N. Cho, Y. F. Wang, and D. R. Chen, "Breast density analysis in 3-D whole breast ultrasound images," Proc. of the 28th IEEE EMBS Annual International Conference (EMBC 2006), 2006, pp. 2795–2798.
[34]R. W. Ehrich, "A symmetric hysteresis smoothing algorithm that preserves principal features," Comput. Graph. Image Process. **8**, 121–126 (1978).
[35]N. Otsu, "A threshold selection method from gray-level histograms," IEEE Trans. Syst. Man Cybern. **SMC-9**, 62–66 (1979).
[36]J. F. Canny, "A computational approach to edge detection," IEEE Trans. Pattern Anal. Mach. Intell. **8**, 679–698 (1986).
[37]S. Yokoi, J. Toriwaki, and T. Fukumura, "An analysis of topological properties of digitized binary pictures using local features," Comput. Graph. Image Process. **4**, 63–73 (1975).
[38]L. Vincent and P. Soille, "Watershed in digital spaces: An efficient algorithm based on immersion simulation," IEEE Trans. Pattern Anal. Mach. Intell. **13**, 583–598 (1991).
[39]Y. L. Huang and D. R. Chen, "Watershed segmentation for breast tumor in 2-D sonograph," Ultrasound Med. Biol. **30**, 625–632 (2004).
[40]K. Fukunaga, *Introduction to Statistical Pattern Recognition*, 2nd ed. (Academic, New York, 1990).
[41]J. Serra, "Introduction to mathematical morphology," Comput. Vis. Graph. Image Process. **35**, 283–305 (1986).
[42]R. A. Johnson and D. W. Wichern, *Applied Multivariate Statistical Analysis* (Prentice-Hall, Englewood Cliffs, NJ, 1992).
[43]S. Theodoridis and K. Koutroumbas, *Pattern Recognition* (Academic, San Diego, CA, 1999).
[44]D. P. Chakraborty, "Maximum likelihood analysis of free-response receiver operating characteristic (FROC) data," Med. Phys. **16**, 561–568 (1989).